



Boundary-Aware and Multiscale Methods for Topology Optimization

Mario Setta

Faculty of Health, Science and Technology

Mathematics

DOCTORAL THESIS | Karlstad University Studies | 2026:31

Boundary-Aware and Multiscale Methods for Topology Optimization

Mario Setta

Boundary-Aware and Multiscale Methods for Topology Optimization

Mario Setta

DOCTORAL THESIS

Karlstad University Studies | 2026:31

urn:nbn:se:kau:diva-109536

ISSN 1403-8099

ISBN 978-91-7867-711-5 (print)

ISBN 978-91-7867-712-2 (pdf)

<https://doi.org/10.59217/xcx4708>

© The author

Distribution:

Karlstad University

Faculty of Health, Science and Technology

Department of Mathematics and Computer Science

SE-651 88 Karlstad, Sweden

+46 54 700 10 00

Print: Universitetstryckeriet, Karlstad 2026

WWW.KAU.SE

Boundary-Aware and Multiscale Methods for Topology Optimization

MARIO SETTA

Department of Mathematics and Computer Science

Abstract

Over the past decades, topology optimization has become a powerful tool for the design of high-performance multi-material structures. However, significant challenges persist when including selected geometric properties of the generated designs into the optimization process. At the same time, research on small electronic devices and advances in additive manufacturing have contributed to the miniaturization of electronic components for increasingly compact and highly performant systems. Under this significant length-scale reduction, classical continuum mechanics loses its accuracy, leaving room for size-dependent effects to occur. In this thesis, we expand on recent developments in boundary-aware formulations, specifically for coated structures, and scale-size dependent modeling for topology optimization.

We introduce a boundary strip indicator based on morphological operators. The proposed indicator defines a mathematically consistent tool for identifying, for example, coating layers. To explore the versatility of the indicator, two different methods have been tested: one based on binary design variables, while the other uses continuous design variables. Numerical experiments showcase the ability of the boundary strip indicator to incorporate a coating layer in the topology optimization process.

To address the lack of accuracy of classical continuum models when approaching the molecular scale, we employ a higher-order theory governed by relative length scales. Within this theory, scale-size effects are captured by higher-order terms in the homogenized fourth-order partial differential equations. This thesis presents a numerical implementation using quadratic B-splines to ensure the required regularity of the equations. Numerical simulations exhibit the influence of different scale-size-dependent properties on selected test domains and on the topology of the optimized microstructures.

Keywords: Topology optimization, size control, nonlinear filters, coated structures, scale-size effects, homogenization, finite element method

Sammanfattning

Under de senaste decennierna har topologioptimering blivit ett kraftfullt verktyg för konstruktion av högpresterande multimaterialstrukturer. Det kvarstår dock betydande utmaningar när det gäller att inkludera specifika geometriska egenskaper hos de genererade konstruktionerna i optimeringsprocessen. Samtidigt har forskning kring små elektroniska enheter och framsteg inom additiv tillverkning bidragit till miniatyrisering av elektroniska komponenter för alltmer kompakta och högpresterande system. Vid denna kraftiga minskning av längdskalan förlorar den klassiska kontinuummekaniken sin validitet, vilket ger upphov till storleksberoende effekter. I denna avhandling bygger vi vidare på den senaste utvecklingen inom randmedvetna formuleringar, särskilt för belagda strukturer (coated structures), och storleksberoende modellering för topologioptimering.

Vi introducerar en randområdesindikator baserad på morfologiska operatörer. Den föreslagna indikatorn utgör ett matematiskt konsistent verktyg för att identifiera exempelvis beläggningsskikt. För att undersöka indikatorns mångsidighet har två olika metoder testats: en baserad på binära konstruktionsvariabler och en som använder kontinuerliga variabler. Numeriska experiment visar på indikatorns förmåga att integrera beläggningsskikt i topologioptimeringsprocessen.

För att åtgärda bristen på noggrannhet hos klassiska kontinuummodeller när den molekylära skalan nalkas, använder vi en teori av högre ordning som styrs av relativa längdskalor. Inom denna teori fångas storlekseffekter upp av termer av högre ordning i de homogeniserade partiella differentialekvationerna av fjärde ordningen. Avhandlingen presenterar en numerisk implementering med kvadratiska B-splines för att säkerställa ekvationernas erforderliga regularitet. Numeriska simuleringar visar hur olika skalberoende egenskaper påverkar utvalda testdomäner och topologin hos de optimerade mikrostrukturerna.

Sommario

Negli ultimi decenni, l'ottimizzazione topologica è diventata uno strumento potente per la progettazione di strutture multimateriali ad alte prestazioni. Tuttavia, integrare determinate proprietà geometriche nel processo di ottimizzazione rimane una sfida significativa. Parallelamente, la ricerca sui dispositivi elettronici miniaturizzati e i progressi nella produzione additiva hanno favorito lo sviluppo di sistemi sempre più compatti e performanti. In virtù di questa drastica riduzione delle scale dimensionali, la meccanica del continuo classica perde la sua validità, lasciando emergere effetti dipendenti dalla dimensione. Questa tesi approfondisce i recenti sviluppi nelle formulazioni per la gestione delle condizioni al contorno, con particolare riferimento alle strutture rivestite (coated) e alla modellazione dipendente dalla scala per l'ottimizzazione topologica.

Viene presentato un indicatore di bordo basato su operatori morfologici. Tale indicatore costituisce uno strumento matematicamente coerente per identificare, ad esempio, gli strati di rivestimento. Per valutarne la versatilità, sono stati testati due metodi: uno basato su variabili di progetto binarie e l'altro su variabili continue. Gli esperimenti numerici dimostrano la capacità dell'indicatore di integrare efficacemente uno strato di rivestimento nel processo di ottimizzazione.

Per ovviare alla perdita di precisione dei modelli classici in prossimità della scala molecolare, viene impiegata una teoria di ordine superiore governata da scale di lunghezza relative. In tale ambito, gli effetti di scala sono catturati da termini di ordine superiore in equazioni differenziali parziali omogeneizzate del quarto ordine. La tesi presenta un'implementazione numerica basata su B-spline quadratiche per garantire la regolarità richiesta dalle equazioni. Le simulazioni numeriche mostrano come le diverse proprietà dipendenti dalla scala influenzino i domini di test e la topologia delle microstrutture ottimizzate.

Acknowledgements

I would like to express my gratitude to everyone who has supported me throughout the development of this work.

First and foremost, I am deeply grateful to my supervisor, Eddie Wadbro, for the insightful discussions and continuous guidance. His expertise and encouragement have been invaluable in shaping this thesis. I am also grateful for the many enjoyable moments shared outside of work, which contributed to a positive and inspiring collaboration.

I would like to acknowledge my colleagues in the Department of Mathematics and Computer Science, where this work was carried out, and the Design Optimization Group for providing a stimulating research environment. In particular, I would like to thank Khanh, Nicklas, Grigor, Surendra, Vishnu, Adrian, Giulia, Linus, Abbas, Juan Carlos, Harry, Ahmad, Pan, Martin, Daniel, Emad, Balaje, and Zach for fruitful conversations and collaborations, and for making a pleasant working environment. I would also like to thank Renato, Rômulo, Lucas, Kamilla, and my colleagues and friends around the world for the enriching exchanges that have contributed to my professional and personal development. Next, I would like to thank my fellow PhD students for creating a stimulating and enjoyable atmosphere throughout this journey. Special thanks go to Phil for his support, engaging discussions, and for contributing to an enjoyable living environment.

On a personal note, I am greatly thankful to my friends for their presence and encouragement throughout this journey. Tommaso, Eleni, Daniele, Nico, Federico, Marialuigia, Leonardo, Celsi, Fredrik, and Klara, thank you for the many memorable and enjoyable moments we have shared. Finally, I would like to express my deepest gratitude to my partner, Julia, for her patience, understanding, and support throughout this process. Last but not least, I am deeply grateful to my family for their continuous love and support. Grazie!

Karlstad, May 5, 2026

Mario Setta

Contents

INTRODUCTORY SUMMARY	1
1 Introduction	3
1.1 Research Questions	4
2 Material-Distribution Topology Optimization	4
2.1 Problem Formulation	5
2.2 Selected Topology Optimization Methods	6
3 Filters and Minimum Size Control [Paper I]	7
3.1 Minimum Size Control for Compliance Problems	8
3.2 Selected Results	9
4 Minimum Heat Compliance for Coated Structures [Papers II and III]	11
4.1 Boundary Strip Indicator	11
4.2 Problem Formulation	12
4.3 Selected Results	13
5 Alternative Boundary-Aware Formulations for Coated Structures [Paper IV]	15
5.1 Gradient-Based Methods	16
5.2 Morphology-Inspired Methods	17
5.3 Image-Inspired Methods	18
6 Scale-Size Dependent Heat Conduction [Paper V]	18
6.1 Motivation	18
6.2 Problem Formulation	18
6.3 Numerical Modeling	20
6.4 Selected Results	22
7 Optimization of Scale-Size Dependent Microstructures	24
7.1 Problem Formulation	24
7.2 Sensitivity analysis	25
7.3 Selected Results	26
8 Concluding Remarks and Future Work	30
List of Appended Papers	33
References	35
PAPER I:	
Minimum size control for binary topology optimization	41

- 1 Introduction 41
- 2 Problem statement 43
 - 2.1 Thermal compliance 43
 - 2.2 Structural compliance 44
- 3 Design encoding 46
- 4 The TOBS method 49
- 5 Numerical experiments and discussion 51
 - 5.1 Minimum thermal compliance 51
 - 5.2 Minimum structural compliance 56
- 6 Conclusion 59
 - 6.1 Integration in Our Work and Applicability 59
- References 60

**PAPER II:
A boundary strip indicator for material distribution-based
topology optimization 67**

- 1 Introduction 67
- 2 Test problem 69
- 3 Boundary strip indicator 71
- 4 Boundary strip as coating layer 75
- 5 Numerical experiments 77
- 6 Discussion and outlook 80
- References 81

**PAPER III:
Binary topology optimization for coated structures 87**

- 1 Introduction 87
- 2 Boundary strip indicator 88
- 3 Coating Test Problem 89
- 4 The TOBS Method 90

5	Numerical results	90
6	Discussion and outlook	93
	References	94

PAPER IV:		
Material distribution topology optimization for boundary-effect-dominated problems: a review		99
1	Introduction	99
2	History of related ideas	102
3	Design description and filtering	105
3.1	Computational complexity and versatility	108
3.2	Cascades of filters and multi-field representations	108
4	Design-dependent pressure load	109
4.1	Parameterized surface methods	110
4.2	Material phase-based methods	113
4.3	Image-based boundary detection	116
4.4	Element-wise boundary tracking	118
5	Design-dependent heat flux	121
6	Coated structures	127
6.1	Gradient-based coating indicators	128
6.2	Morphology-inspired methods	131
6.3	Image-inspired boundary detection	135
7	Problems with layers	137
8	Concluding discussion	143
	References	148

PAPER V:		
Simulation of effective scale-size dependent heat conduction in rigid microgeometries		165
1	Introduction	165
2	Thermodynamic modeling	167
2.1	Conservation of mass	167
2.2	Balance of linear momentum	168
2.3	Balance of angular momentum	168

- 2.4 Entropy contribution to the mechanical work 168
- 2.5 First law of thermodynamics 169
- 2.6 Second law of thermodynamics 169
- 2.7 Rigid heat conductor 170
- 2.8 Approximation of the energy response function 171
- 2.9 An additional length scale modeling thermal scale-size effects . . . 172

- 3 Multiscale analysis of a prototype diffusion with scale-size thermal effects 173**
 - 3.1 The multiscale structure of the heterogeneous medium 173
 - 3.2 Scaling of the variables 174
 - 3.3 Slip length comparable to the size of the heterogeneity 175
 - 3.4 Homogenization via two-scale expansion for the steady state enhanced heat equation 176

- 4 Numerical modeling 178**

- 5 Numerical simulations 181**
 - 5.1 Accuracy study 181
 - 5.2 Scale effect study 182

- 6 Concluding remarks 187**

- References 188**

Introductory Summary



1 Introduction

Designing highly performant systems in an efficient way is one of the main challenges of product development. Traditional design engineering relies on experience, prior knowledge, and intuition to develop suitable and potentially performant systems. This results in a workflow that is generally time-consuming and limiting. Computational design optimization is the field that combines simulations with numerical optimization to generate designs that maximize system performance. Generally, computational design optimization can employ several constraints, different optimization techniques, and it is usually faster than the traditional counterpart.

From the broad realm of computational design optimization methods, we consider topology optimization. Topology optimization encompasses a set of powerful tools capable of combining design, physics, and constraints by systematically determining a material distribution that optimizes a prescribed objective. Over the years, the applications of topology optimization have evolved from structural mechanics to, among other problems, heat propagation, multiphysics systems, boundary-dependent systems, and microscale problems.

With the growing interest in computational design optimization methods, increasingly complex problems can be tackled with innovative topology optimization techniques. Despite recent developments in the field, substantial challenges remain in applying topology optimization to problems where certain geometric features and physical effects are strictly coupled. On the one hand, additional care is needed for an accurate representation of boundaries and interfaces to integrate perimeter constraints, boundary-dependent loads, or coated structures into the optimization process. On the other hand, advances in manufacturing techniques favoured a length-scale reduction of producible systems. At such small scales, classical continuum models are insufficient, as the physical properties of the system explicitly depend on the characteristic length of system components.

This thesis explores the challenges of developing a computational framework that accounts for the described geometrical and physical effects. Heat conduction problems serve as a test ground for the proposed methods, providing an intuitive setup to investigate the system's behavior. The work is organized around two main research directions.

The first research direction regards boundary-aware methods in topology optimization. Here, the aim is to build a mathematically sound method for the unambiguous identification of a strip of fixed thickness along the boundary of the design. Using concepts from mathematical morphology, a boundary strip indicator is introduced. By building a suitable differentiable approximation of the indicator, we ensure its applicability to gradient-based optimization methods. The boundary strip indicator is finally used to include a coating layer in the design process. Moreover, other existing boundary-aware methods are studied.

The second research direction focuses on incorporating scale-size effects into heat propagation for materials with rigid microstructures. When characteristic lengths become small, and classical Fourier's law fails to capture the experimental behavior, a higher-order theory is needed. This results in an enhanced differential

equation containing size-dependent higher-order terms. Taking into account the required smoothness, we present a homogenization and numerical framework to compute the effective properties of such microstructures. Finally, the design of size-dependent microstructures is optimized with respect to some prescribed objective and requirements.

To demonstrate the applicability of these developments, different gradient-based optimization methods are implemented. The numerical results show the flexibility of topology optimization to incorporate diverse modeling features, such as coating layers and scale-size effects. A central theme emerging from the resulting designs is the importance of incorporating such features throughout the optimization process.

1.1 Research Questions

This thesis encompasses the development and analysis of beyond state-of-the-art computational design optimization algorithms and methods. These methods will be used to solve practical problems, such as heat propagation. The proposed studies are divided into two main parts: investigating geometric properties, in particular, boundary identification and treatment in compliance problems; and formulating a modeling and numerical framework to include size-dependent effects into heat conduction in rigid microgeometries. Therefore, we will develop efficient gradient-based design optimization methods based on the developed approaches. The research questions that we tackle throughout this thesis are:

1. *How can we extend the theory of morphological operators to develop approximate morphological operators for minimum size control and boundary identification?*
2. *Do these morphological operators-based methods enable rigorous geometric handling to solve boundary-effect dominated heat-compliance problems?*
3. *How can we accurately solve heat conduction equations containing scale-size dependent effects in rigid microgeometries?*
4. *Can scale-size dependent effects be incorporated into the design optimization of microstructures?*

2 Material-Distribution Topology Optimization

The term *topology optimization* encompasses a set of computational design methodologies used to determine the material distribution that optimizes the performance of a physical system, within a design domain, subject to some prescribed conditions and penalty functions. Generally, an objective function describes the performance of the system, which is subject to physical and manufacturing constraints [Bendsøe and Sigmund, 2003].

The 1971's paper by Lions on optimal control for partial differential equations was one of the primary inspirations for the development of the design optimization field [Kohn and Strang, 1986a,b,c]. However, modern topology optimization originates from the work by Bendsøe and Kikuchi [1988] in structural engineering.

Since then, topology optimization has evolved into a mature discipline with applications in different fields, including but not limited to heat transfer, fluid-structure interaction, and other multi-physics systems. Nowadays, topology optimization is broadly employed in the design process of components in sectors such as structural engineering, aerospace, naval, and automotive.

This section serves as a brief introduction to the mathematical formulation and the techniques used in this thesis.

2.1 Problem Formulation

We start by considering, in a binary setup, a material indicator ρ over a design domain $\Omega \subset \mathbb{R}^d$, such that $\rho = 0$ indicates the absence of material and $\rho = 1$ the presence of material. A common approach is also to relax the material indicator to a material distribution function, that is, we allow continuous values of $\rho \in [0, 1]$. The distinction between binary and continuous design variables and their respective roles in this thesis will be discussed in more detail later. Similarly, the governing physics is kept abstract to provide a generalized presentation of the topology optimization framework; specific test cases will be presented as needed.

We suppose the physics of the considered system to satisfy the variational problem: for U and V appropriate function spaces, find $u \in U$, such that

$$a_\rho(u, v) = \ell(v) \quad \forall v \in V. \quad (1)$$

As a consequence of this formulation, the state variable u implicitly depends on the design variable ρ . Formally, a generic topology optimization problem can be written as

$$\begin{cases} \min & J(u, \rho) \\ \text{subject to} & \text{Equation (1),} \\ & \text{additional constraints,} \end{cases} \quad (2)$$

where $J(u, \rho)$ is the objective function, and the additional constraints could stem from a physical or manufacturing standpoint.

To numerically solve the above optimization problem, we discretize the design domain into small elements, and we let ρ_h be an element-wise constant approximation of ρ . Let $U_h \subset U$ and $V_h \subset V$ be appropriate discretizations of U and V , respectively. Thus, let us define $u_h \in U_h$ and $v_h \in V_h$ the discretized versions of u and v , respectively. Then, for a_{h,ρ_h} and ℓ_h the discretized versions of a_ρ and ℓ , the discretized variational problem reads as: find $u_h \in U_h$, such that

$$a_{h,\rho_h}(u_h, v_h) = \ell_h(v_h) \quad \forall v_h \in V_h. \quad (3)$$

Here, the lower bound for ρ_h is usually changed into a small value ϵ to ensure the existence and uniqueness of the numerical solutions. Therefore, for J_h , the discretized objective function J , the discretized optimization problem is:

$$\begin{cases} \min & J_h(u_h, \rho_h) \\ \text{subject to} & \text{Equation (3),} \\ & \text{additional constraints.} \end{cases} \quad (4)$$

Without suitable regularization, the designs attained by solving problem (4) may exhibit mesh dependence and numerical artifacts such as checkerboard patterns. Moreover, if the relaxed design variable is selected, one wants the final design to be as close to binary as possible. The *gray areas* in the design, meaning where $\rho_h \in (0, 1)$, can be quantified by the measure of non-discreteness (M_{nd}) proposed by Sigmund [2007]. Here, $M_{nd} = 0\%$ indicates the design to be completely binary, while $M_{nd} = 100\%$ indicates the design to be totally gray, that is, $\rho_h = 0.5$ in all the elements.

In this thesis, we address these known issues by operating a filtering strategy based on harmonic filters [Svanberg and Svård, 2013]. We will explore some filters and their application in more detail later in this section. To support the filtering strategy, we employ the Solid Isotropic Material with Penalization (SIMP) method. The SIMP method, firstly introduced by Bendsøe [1989], provides a powerful tool to push the design towards a binary one, and to interpolate the physical material properties in Equation (3). Thus, both the filtering strategy and the penalization are coupled with an appropriate continuation approach on the methods' parameters [Tovar and Khandelwal, 2011]. Several other strategies to resolve these issues have been proposed over the years. The interested reader can find an exhaustive review of classic restriction methods in Borrvall's [2001] article.

At this point, the ingredients one needs for solving problem (4) are: a parametrization of choice for the material distribution (binary or relaxed); a solver for the variational problem to evaluate the state variables; sensitivity analysis (that we perform via the adjoint methods); filtering and penalization combined with a suitable continuation method; an appropriate method for updating the design (depending on the chosen parametrization and the problem kind). We shall now explore some methods used in the development of this thesis.

2.2 Selected Topology Optimization Methods

Here, we follow two different gradient-based approaches to solve the above nonlinear integer programming problem: linearize it and solve it with a binary method, or relax the design variable to allow intermediate values, that is, $\rho \in [0, 1]$. Let us briefly explore the two cases.

To solve problem (2) with a binary method of our choosing, that is, the Topology Optimization of Binary Structures (TOBS) method proposed by Sivapuram and Picelli [2018], we linearize the objective function and the constraints following the Sequential Approximate Integer Programming (SAIP) method Liang and Cheng [2019]. The SAIP method breaks down the problem into a series of Integer Linear Programming (ILP) sub-problems, which are solved using a branch-and-bound algorithm. The major distinction over the more popular Bi-directional Evolutionary Structural Optimization (BESO) developed by Querin et al. [1998] is in the ability of the TOBS method to handle multiple non-volume constraints. The TOBS method provides a completely discrete design, but needs tuning of parameters and has a high computational cost, being ILP NP-complete [Rabiner, 1984]. However, the problem can be solved quite efficiently with commercial software, like CPLEX [IBM Corporation, 2022]. In this thesis, we employ the

TOBS method in Papers I and III.

On the other hand, to solve the relaxed version of problem (2) with $\rho \in [0, 1]$, we rely on two methods: the Optimality Criteria (OC) method or the Method of Moving Asymptotes (MMA). The idea behind the OC method is to build an iterative method that updates the design variables according to the necessary conditions of optimality [Bendsøe, 2013]. The update step is handled via closed-form expressions based on computed sensitivities and Lagrange multipliers. Sigmund [2001] provides a clear description of the method for a minimum compliance problem and its Matlab implementation. Alternatively, we can use the MMA originally formulated by Svanberg [1987] to construct and solve a sequence of convex, separable subproblems approximating the original problem. Thus, the method uses adaptive asymptotes to update the design variables according to sensitivities at the current iteration as well as iteration history. Since then, a globally convergent version of the MMA (GCMMA) has been developed by Svanberg [2002]. However, the problems we will tackle are simple enough to choose the faster MMA over the more conservative, robust, and computationally demanding GCMMA. While the OC method is simple and particularly effective for compliance problems, the MMA improves in convergence properties for more complicated problems with several prescribed constraints. In this thesis, we employ the OC method in Paper II. Moreover, we use the MMA for a paper currently in preparation, with preliminary results presented in Section 7.

3 Filters and Minimum Size Control [Paper I]

Throughout the evolution of topology optimization, many regularization techniques and restriction methods have been proposed to reduce mesh dependence and unwanted artifacts such as checkerboard patterns in the resulting designs. Sigmund [1994] provides one of the earliest applications of filtering techniques to prevent unwanted checkerboard patterns. There, the design is interpreted as a digital image, and denoising techniques from digital image processing are used to mitigate isolated pixel variations. More broadly, Borrvall [2001] provides a comprehensive study of commonly used restriction methods. Beyond suppressing unwanted artifacts, some restriction methods are also used to enforce a minimum size on the design's topological details, ensuring manufacturability. In this section, we briefly explore a methodology based on morphological operators, approximated by means of fW -mean filters [Wadbro and Hägg, 2015], and how it can help control minimum size in the optimization process.

The history of filtering techniques based on morphological operators traces back to Minkowski's [1903] studies on spatial set algebra and Matheron's [1974] work on topology. Mathematical morphology was originally defined for sets. Namely, for a set M and a structuring element B , the erosion and dilation morphological operators were defined as the Minkowski difference $M \ominus B$ and sum $M \oplus B$, respectively. From there, mathematical morphology expanded its applicability with the advent of digital images for the development of digital image processing techniques [Pratt, 1991]. Thus, the definition naturally extends to binary or gray-scale images, which is how we represent our design ρ over a bounded

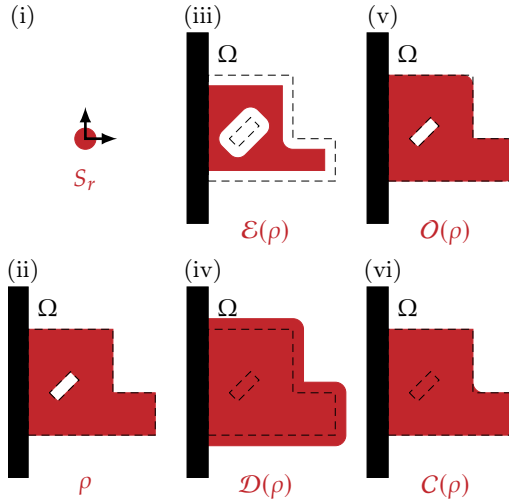


Figure 1: Example of the erode (iii), the dilate (iv), the open (v), and the close (vi) morphological operators applied to a binary test design (ii). The radius r of the ball S_r in (i) indicates the radius of the operators. Figure from Paper I.

domain.

Consider a design ρ over a design domain $\Omega \subset \mathbb{R}^n$ and let the structuring element $S_r(x)$ be a ball of radius r centered in $x \in \Omega$. In this case, the erode $\mathcal{E}(\rho)$ and the dilate $\mathcal{D}(\rho)$ morphological operators can be seen as min and max operators, respectively [Hägg and Wadbro, 2018]. Moreover, we consider the open $\mathcal{O}(\rho)$ and close $\mathcal{C}(\rho)$ morphological operators as the combination of erode and dilate operators. Intuitively, the erode operator cuts a strip from the border of the design. On the other hand, the dilate operator adds a strip to the design's border. The structuring element's radius determines the width of this strip. Figure 1 displays how the erode (iii), the dilate (iv), the open (v), and the close (vi) morphological operators, with structuring element S_r (i), act on the test design (ii).

Unfortunately, min and max operators are not differentiable, and the morphological operators need to be properly approximated to enable gradient-based optimization. Here, we consider harmonic filters as suitable approximations of the morphological operators. For more information about these filters, we refer the reader to the work by Svanberg and Svärd [2013] and by Wadbro and Hägg [2015]. Moreover, Sigmund [2007] provides a broad survey of morphology-inspired filters. We shall now briefly explore how to use these filters to enforce minimum size control, with a focus on minimum compliance problems.

3.1 Minimum Size Control for Compliance Problems

To achieve minimum size control (often referred to as minimum length-scale control), we first need to understand how the minimum length-scale property is

defined. Here, we consider the definition from Hägg and Wadbro [2018], denoted NEighborhood based minimum Length scale (NEL). Let us define the material phase to be the area of the design variable where $\rho = 1$, and a sphere S_r with radius r (for example, the red area of (ii) and the structuring element (i) in Figure 1, respectively). Then, the NEL states that a material phase possesses a minimum length scale of r if and only if any point of the material phase belongs to a sphere S_r completely contained in the material phase. Zhang et al. [2014] provide a more detailed definition based on the identification of a structural skeleton of the material, which is probed with a closed sphere \bar{S}_r .

Conceptually, different combinations of filters can be employed to impose minimum size control. For example, for a structuring element of radius $r > 0$, the closed morphological operator provides a minimum length scale of r to the material phase. Similarly, the open operator provides a minimum length scale of r to the void phase. Importantly, a design ρ satisfying the equality

$$O(\rho) = C(\rho) \quad (5)$$

possesses a minimum length scale of r on both the material and the void phases. To quantify how close a design ρ is to achieving minimum size control, we employ a quality measure based on the fraction of the design where the difference between $O(\rho)$ and $C(\rho)$ is greater than a cutoff value.

Furthermore, a useful pointwise property of these operators is that

$$O(\rho) \leq \rho \leq C(\rho). \quad (6)$$

The strategy to achieve equality (5) is to penalize any design with $O(\rho) \neq C(\rho)$, pointwise. In the context of volume-constrained minimum compliance problems, where adding material would lower the objective value, the heuristic is to compute compliance using the open filtered design and the close filtered design for the volume constraint. According to inequality (6), the heuristic suggests that those regions where $O(\rho) \neq C(\rho)$ provide a small contribution to minimizing the objective, at the cost of a significant contribution in the volume, thus promoting regions with minimum length-scale control. The detailed study of the heuristic's applicability on binary design optimization for structural and thermal compliance problems can be found in Paper I.

3.2 Selected Results

To test the capability of the filtering strategy to enforce minimum size control, we consider standard benchmark problems commonly found in the literature: minimizing the structural compliance of a cantilever beam and the thermal compliance. Both problems are solved using the Topology Optimization of Binary Structures (TOBS) method [Sivapuram and Picelli, 2018].

Let Ω be a design domain partitioned into $n = n_x \times n_y$ square elements, and let $\rho \in \{0, 1\}^n$ be an elementwise constant material distribution. Domain dimensions are set to $L \times 3L/2$ for the cantilever case and $L \times L$ for the thermal problem.

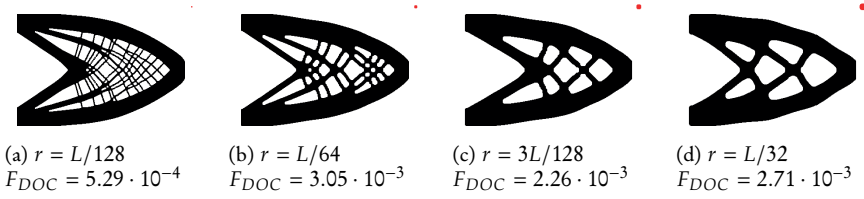


Figure 2: Resulting designs for the structural problem with varying filter radius r and relative compliance values. A red circle next to each topology indicates the filter radius size. Figure from Paper I.

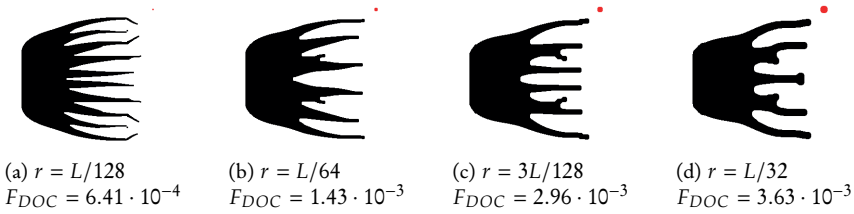


Figure 3: Optimized designs for minimal thermal compliance for varying filter radii r . The red region next to each design depicts the used filter kernel's shape and size. Figure from Paper I.

To measure the ability of this method to impose minimum size control, we employ a quality measure indicating the fraction of elements where the difference between $\hat{O}(\rho)$ and $C(\rho)$ is greater than a cutoff value of 0.5. Specifically, the quality measure can be stated as

$$F_{DOC} = \frac{\text{card}\{i \mid (C(\rho) - \hat{O}(\rho))_i > 0.5\}}{n}. \quad (7)$$

Figure 2 and Figure 3 show the optimized designs for the structural and thermal problems, respectively. The red circle on the top right of each design indicates the radius of the structuring element S_r . Below each figure, the used filter radius and the value of the quality measure F_{DOC} are indicated. Upon visual inspection of the optimized designs, there appear to be no features smaller than their respective structuring elements. The low magnitude of the quality measure supports the visual suggestion, indicating that only a small fraction of elements differ between the open- and close-filtered designs. This result verifies that the final designs successfully achieve minimum size control.

4 Minimum Heat Compliance for Coated Structures [Papers II and III]

In many systems, performance depends not only on the bulk material design but also on interfaces and boundary effects. Coated structures are a particular example of these systems, where designing the bulk material alone is insufficient. Such composite structures are relevant, for example, when the system needs a reinforcement layer, corrosion protection, or thermal shielding.

To incorporate these effects in the design of coated structures, the substrate and the coating layer must be considered simultaneously. In material distribution topology optimization, the treatment of these composite structures poses significant challenges. To address these challenges, we focus on a boundary-aware formulation that enables a non-ambiguous identification of a strip along the boundary of the design. By integrating geometric information—such as the boundary location and the thickness of the desired layer—into the optimization problem, we can model coated structures consistently.

In this section, we introduce a boundary strip indicator capable of identifying a coating layer along the boundary of the design. Successively, the indicator is tested on a thermal dissipation problem. To test the applicability of the proposed indicator, we solve the optimization problem using the Optimality Criteria (OC) method [Bendsøe, 2013] for relaxed design variables and the Topology Optimization of Binary Structures (TOBS) method [Sivapuram and Picelli, 2018] for binary ones.

4.1 Boundary Strip Indicator

Assume ρ to be a design (relaxed or binary) over a design domain $\Omega \subset \mathbb{R}^n$. To define a suitable identifier for coating layers using the morphological operators described in Section 3. We now explore how to identify the substrate and the coating layer of a coated structure defined by the design ρ .

Let the structuring element $S_r(\mathbf{x})$ be a ball of radius r centered in $\mathbf{x} \in \Omega$. Building on the morphological operators shown in Figure 1, we identify the substrate with the eroded design $\mathcal{E}(\rho)$. Therefore, we define the boundary strip indicator as

$$\mathcal{B}(\rho) = \mathcal{D}(\rho) - \mathcal{E}(\rho). \quad (8)$$

The benefit of the above formulation is that, for (almost) binary designs, there is (almost) no overlap between the substrate and the coating layer. The non-negativity of the proposed indicator guarantees this property. Paper II studies this and other relevant properties of the boundary strip indicator.

Figure 4 displays the boundary strip indicator (iii) computed on a binary test design ρ (ii) with structuring element S_r . We note that the strip thickness is directly determined by the diameter of the structuring element, $2r$. To allow gradient-based optimization, we approximate the boundary strip indicator using fW -mean filters [Wadbro and Hägg, 2015], implying that we do not introduce any additional tuning parameters, since the indicator relies only on the filters' radius and non-linearity parameter, as in other standard filtering techniques.

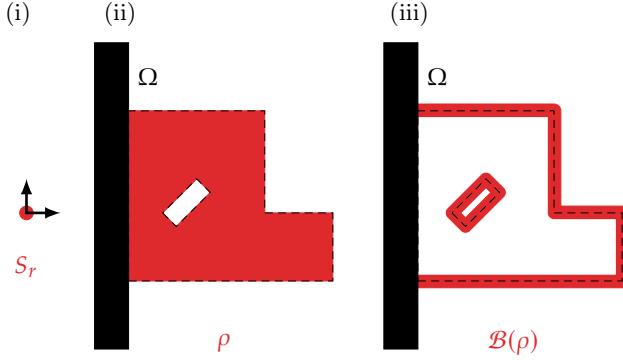


Figure 4: Binary test-case design ρ (ii) and its respective boundary strip indicator $\mathcal{B}(\rho)$ (iii), assuming there is material outside of the design domain on the left side (in black). Here, the radius r of the structuring element S_r in (i) indicates the radius of the operators. Figure from Paper II.

4.2 Problem Formulation

To test the proposed boundary strip indicator, we introduce a modified version of the standard minimum thermal compliance problem. By modifying the material interpolation, we implement the boundary strip as a coating layer to simultaneously optimize both components of the composite structure.

Consider the domain Ω as shown in Figure 5, where we impose that fixed material is on the left of the domain (in gray). Moreover, we impose thermal insulation along the boundary portion Γ_N , we set the temperature to zero along the portion Γ_D , and we let the domain Ω be subject to uniform heating. Then, the steady-state heat propagation can be described by the following variational problem: find $u \in U$, such that

$$\int_{\Omega} P_c(\rho) \nabla u \cdot \nabla v = \int_{\Omega} v, \quad \forall v \in U, \quad (9)$$

where U is an appropriate function space, and $P_c(\rho)$ is the physical thermal conductivity interpolating the properties of the coated structure. We formulate the minimum compliance problem as:

$$\begin{cases} \min & J(u, \rho) = \int_{\Omega} u \\ \text{subject to} & u \text{ satisfies problem (9),} \\ & \mathcal{V}_c(\rho) \leq \mathcal{V}_{\max} \\ & 0 \leq \rho \leq 1, \end{cases} \quad (10)$$

where $\mathcal{V}_c(\rho) \leq \mathcal{V}_{\max}$ is a volume-inspired constraint limiting the total cost of the coated structure.

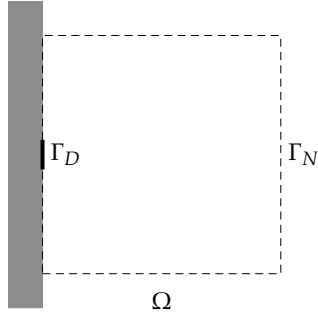


Figure 5: Design domain considered for the solution of the test problem. Here, the boundary consists of two parts: Γ_D , the portion employing homogeneous Dirichlet boundary conditions, and Γ_N , the portion with homogeneous Neumann boundary conditions. We assume to have material (in grey) on the left side of the domain. Figure from Paper II.

To define the physical thermal conductivity and the cost function, we introduce two gain parameters that express the difference in properties of the coating and the substrate. Namely, we define the conductivity gain $\kappa_{\text{gain}} > 0$ as the ratio of the thermal conductivity of the coating, κ_c , and that of the substrate, κ_s . A SIMP-inspired interpolation scheme expresses the physical thermal conductivity of the coated structure as

$$P_c(\rho) = \underline{\rho} + (1 - \underline{\rho})(\mathcal{E}(\rho))^p + (\kappa_{\text{gain}} - \underline{\rho})(\mathcal{B}(\rho))^p, \quad (11)$$

where $p > 1$ is a penalization parameter, and the minimum physical thermal conductivity $\underline{\rho} > 0$ ensures that the equilibrium temperature u is uniquely defined by (9). We define the cost gain $C_{\text{gain}} > 0$ in a similar fashion by dividing the relative cost of the coating, c_c , by that of the substrate, c_s . Therefore, the total cost \mathcal{V}_c of the coated structure assumes the form of a weighted volume constraint as

$$\mathcal{V}_c(\rho) = \frac{1}{|\Omega|} \int_{\Omega} (\mathcal{E}(\rho) + C_{\text{gain}}\mathcal{B}(\rho)). \quad (12)$$

4.3 Selected Results

To test the indicator's ability to model coated structures, we solve optimization problem (10) using both relaxed and binary design variables. Accordingly, we solve the relaxed problem with the OC method, and the binary counterpart with the TOBS method, to examine the effects of the gain parameters and of the layer's thickness on the resulting designs.

For the numerical simulations, we divide the square domain Ω of side L into 256×256 square elements. However, the selected topology optimization

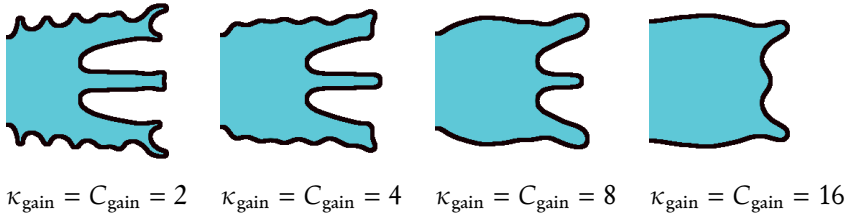


Figure 6: Final design having substrate in cyan and coating layer in black. Here, we vary the gain parameters, namely $\kappa_{\text{gain}} = C_{\text{gain}} = 2, 4, 8, 16$, keeping a fixed filter radius of $L/64$. Figure from Paper II, results attained with the OC method.

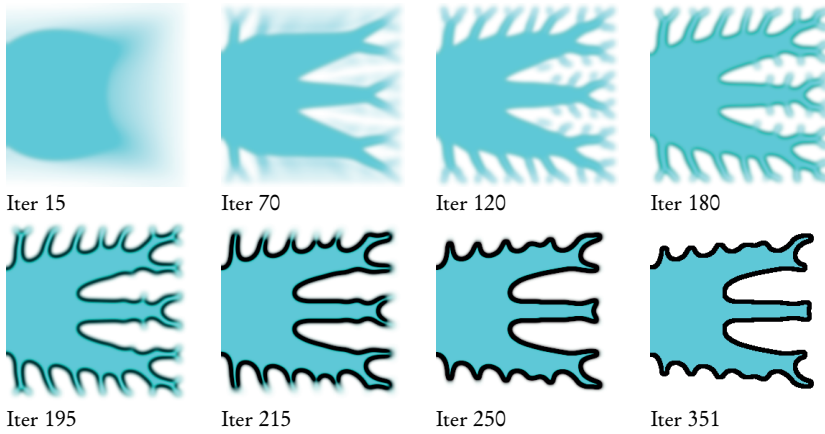


Figure 7: Evolution of the simulation fixing the parameters to $r = L/64$ and $\kappa_{\text{gain}} = C_{\text{gain}} = 2$. Figure from Paper II, results attained with the OC method.

methods rely on different tuning parameters. In the relaxed problem, grey-scale-free final designs are promoted by employing a continuation method [Tovar and Khandelwal, 2011] to adjust the penalization and filter non-linearity parameters gradually. On the other hand, the binary optimization problem is governed by the tuning parameters of the TOBS method. The values chosen for the results in this section are described in Paper II and Paper III, together with more details on the numerical results. In the selected figures below, a white–cyan color scale marks the layout of the substrate $\mathcal{E}(\rho)$, while a white–black color scale marks the layout of the coating, $\mathcal{B}(\rho)$, where white corresponds to void in both color scales.

The first experiment studies the effects of the gain parameters on the final designs using relaxed design variables and the OC method. Fixing the filter radius at $L/64$, we test composite structures in which the coating layer is more conductive and expensive than the substrate. Figure 6 shows the optimized designs for $\kappa_{\text{gain}} = C_{\text{gain}} = 2, 4, 8$, and 16. Furthermore, Figure 7 displays the evolution of the simulation for $r = L/64$ and $\kappa_{\text{gain}} = C_{\text{gain}} = 2$. Here, we identify a

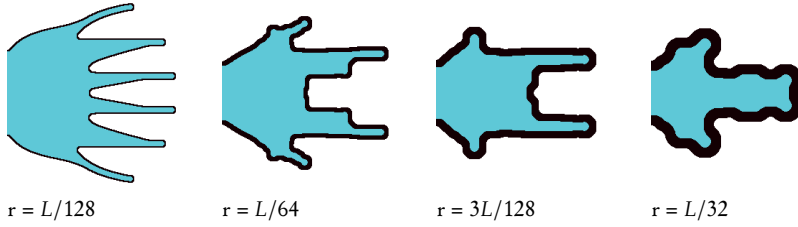


Figure 8: Here, we vary the filter radius, keeping $\kappa_{\text{gain}} = C_{\text{gain}} = 2$. Cyan represents the substrate, and black represents the coating layer. Figure from Paper III, results attained with the TOBS method.

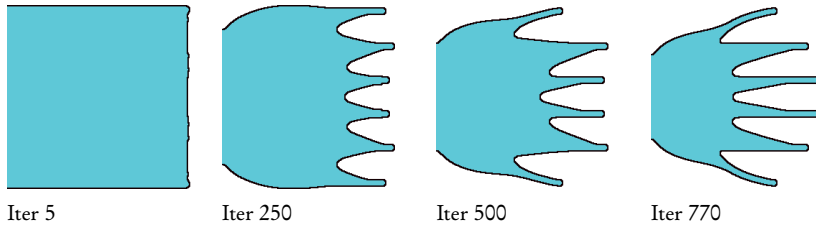


Figure 9: Evolution of the design for filter radius $r = L/128$, and $\kappa_{\text{gain}} = C_{\text{gain}} = 2$ at iterations 5, 250, 500, and the final design at iteration 770. Cyan represents the substrate, and black represents the coating layer. Figure from Paper II, results attained with the OC method.

direct consequence of using relaxed design variables. During the initial iterations, the design is too far from binary to identify a sharp boundary strip visually. Nonetheless, the coating still influences the evolution of the designs from the first steps of the simulations.

Next, we study the effect of the coating's thickness on the final designs using binary design variables and the TOBS method. Figure 8 displays the optimized designs for fixed gain parameters $\kappa_{\text{gain}} = C_{\text{gain}} = 2$, and filter radius $r = L/128$, $L/64$, $3L/128$, and $L/32$. Moreover, we observe the evolution of the optimization process for filter radius $r = L/128$, and $\kappa_{\text{gain}} = C_{\text{gain}} = 2$ at selected iterations in Figure 9. Unlike relaxed design variables, binary design variables allow a clear, sharp coating layer from the first iteration.

5 Alternative Boundary-Aware Formulations for Coated Structures [Paper IV]

Boundary-aware formulations have received increasing attention in topology optimization due to the important role boundary-dependent loads, interfaces, or thin boundary layers can play in the system's physics and performance. The growth of this field is demonstrated through Scopus publication trends for design optimization problems involving design-dependent pressure loads, boundary layers, and

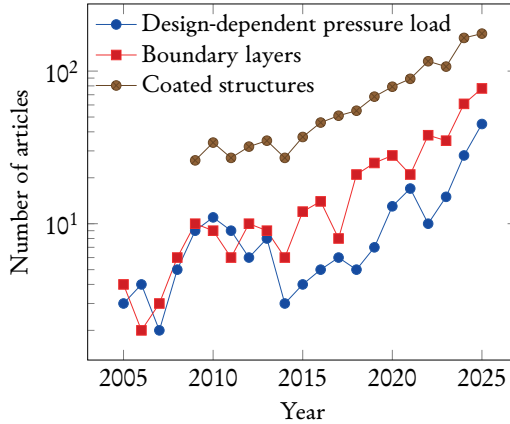


Figure 10: Number of publications per year in the past 20 years for design optimization problems with design-dependent pressure load, boundary layers, or coated structures. Figure from Paper IV.

coated structures. Figure 10 illustrates the growth in interest in boundary-effect-dominated problems over the past two decades, measured via annual publications. The data displayed covers a broad range of design optimization approaches, including density-based, level-set, and classical shape optimization methods.

Paper IV presents a review of boundary-effect-dominated problems in material distribution topology optimization. In this section, we briefly explore selected methods for coated structures, which constitute the part of the work I led in terms of both research and writing.

While the boundary strip indicator introduced in Section 4.1 provides one approach for representing and optimizing coating layers, it is part of a broader class of methods developed to incorporate coatings within material distribution formulations. Existing approaches for modeling such composite structures can be divided into three main categories: gradient-based, morphology-inspired, and image-inspired methods.

5.1 Gradient-Based Methods

A first class of methods identifies coating layers by computing spatial variations in the design field. The underlying idea is that large gradients naturally occur near material interfaces, making the gradient norm a suitable indicator of boundary regions.

A seminal method is the two-step filtering approach proposed by Clausen et al. [2015]. To extract the coating, the design is processed with a PDE filter and scaled with a tanh-based approximation of a shifted Heaviside function. Finally, the coating is identified by scaling the filtered field's gradient, enabling separate control of substrate and coating length scales. For a one-dimensional test-case design field ρ , Figure 11 shows the workflow described above for identifying the

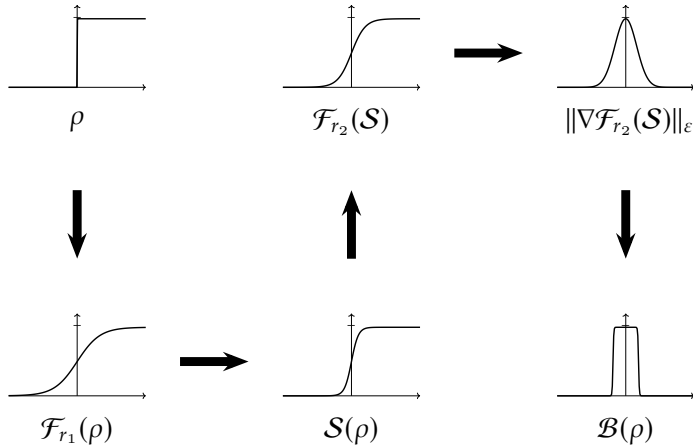


Figure 11: Two-step filtering workflow as described by Clausen et al. [2015]. The normalized gradient of the processed one-dimensional test-case design ρ is scaled to identify the coating layer $\mathcal{B}(\rho)$. Figure from Paper IV.

boundary $\mathcal{B}(\rho)$. There, \mathcal{F}_r indicates a PDE filter of radius r , \mathcal{S} is the shifted Heaviside approximation, and $\|\cdot\|_\epsilon$ is a scaled norm. The use of a double filtering approach with two distinct radii enables independent control of the characteristic length scales of the substrate and the coating. This decoupled regularization has motivated several extensions and applications.

Gradient-based approaches often provide clear formulations and direct sensitivity information. However, they may introduce additional computational overhead through multiple filtering steps and gradient evaluations, and can be sensitive to discretization or parameter tuning.

5.2 Morphology-Inspired Methods

An alternative class of methods is inspired by mathematical morphology. Rather than relying on gradient information, these approaches rely on a combination of the morphological operators described in Section 3 to geometrically identify coating layers.

The identification of the coating layer is usually formulated as a geometric subtraction: the layer is recovered as the difference between an enlarged version of the initial design and a filtered internal infill. This construction offers an intuitive way for modeling a coating layer with a prescribed thickness. Such approaches often provide more effective geometric control over the coated structure than their gradient-based counterparts while avoiding the computational overhead of gradient norms. The boundary strip indicator proposed in Section 4.1 falls into this class of methods.

5.3 Image-Inspired Methods

More recently, image processing techniques have been employed for boundary identification in topology optimization. In particular, these image-inspired methods incorporate low-level image processing techniques to detect structural contours within the material distribution.

An example of low-level image processing is the Smallest Univalued Segment Assimilating Nucleus (SUSAN) algorithm developed by Smith and Brady [1997]. To facilitate precise geometric identification, Postigo et al. [2024] employ the SUSAN algorithm to identify boundary edges based on local density similarities between neighboring elements. Thus, the coating layer can be identified by replacing the gradient norm computation with the SUSAN algorithm in the two-step filtering shown in Section 5.1.

Compared with gradient- or morphology-based formulations, these methods offer a different approach to coating identification. This may be particularly favourable for complex geometries or when the interest is the contour detection. Although some image-inspired methods remain relatively unexplored, they suggest a promising integration of image analysis and topology optimization.

6 Scale-Size Dependent Heat Conduction [Paper V]

In this section, we explore the formulation and numerical modeling of an enhanced heat equation to take into account effective scale-size dependent properties in rigid microstructures. The theory and results presented here are part of the published Paper V. This section also serves as an introduction to some preliminary results of a topology optimization problem for the aforementioned microstructures, presented later on in Section 7. The abundance of detail in this section ensures a self-contained presentation of the subsequent optimization.

6.1 Motivation

Over the past decades, the miniaturization of electronic components has constituted a major focus of research and technological development of increasingly compact and high-performance systems. In parallel, advancements in additive manufacturing techniques have made this length-scale reduction possible in device components. However, as these dimensions approach the molecular scale, significant challenges arise. At such scales, the fundamental assumptions of classical continuum mechanics, like the hypothesis of scale-invariant material properties, lose their accuracy. Thus, size-dependent effects emerge, substantially altering the effective behavior of these devices. Christov [2007], Bauer et al. [2017], Kadic et al. [2018], Ganghoffer et al. [2025a,b].

6.2 Problem Formulation

Let $\Omega \subset \mathbb{R}^2$ be a domain of size L and let Y_m be a periodic microscopic cell of size ℓ and period $\varepsilon := \ell/L \ll 1$, containing m^2 periodic microstructures. Moreover, let $x \in \Omega$ be the macroscopic space variable and $\mathbf{y} \in Y_m$ be the microscopic space

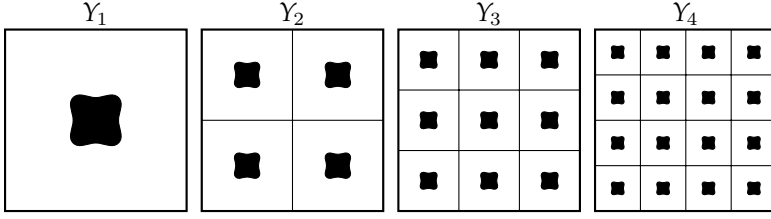


Figure 12: Four possible microscopic periodic unit cells Y_m , where m^2 indicates the number of microstructures in the cell. Figure from Paper V.

variable such that $\mathbf{y} = \mathbf{x}/\varepsilon$. Finally, let ℓ_s be the absolute size of the constituents, that is, the characteristic length scale of a microstructure contained in Y_m . Figure 12 shows the difference between the number of microstructures contained in Y_m , for $m = 1, 2, 3$, and 4. When the absolute size of the constituents scales with the size of the microscopic cell, that is $\ell_s \sim \ell$, mesoscale size effects emerge. To take into account these mesoscopic effects in the macroscopic equations, the effective properties of the macroscopic object contain higher-gradient terms depending on the absolute size of the microstructure [Forest et al., 2001]. It has been shown experimentally by Molavitabrizi et al. [2023] that a relative scale $\ell_s/\ell \sim 1/56$ ensures strict scale separation, nullifying the second-gradient effects.

The enhanced heat equation is derived with the principle of virtual work, which states that the sum of internal, external, and inertial forces acting on any subdomain must vanish for any admissible virtual trial function. The derivation follows the microforce balance [Gurtin, 1996] to incorporate additional contributions of the entropy to the mechanical work as in the work of Forest and Amestoy [2008]. Building on these balance equations, constitutive relations are derived following the well-established Coleman–Noll procedure [Noll and Coleman, 1974]. Finally, for a rigid heat conductor, we attain a fourth-order heat conduction equation in terms of the entropy density capable of modeling scale-size effects. In the steady-state case, we consider the entropy density s_ε . The enhanced heat conduction, depending on micro- and macroscopic scales, is described by

$$\begin{aligned}
 -\operatorname{div} \left(\mathbf{K}(\mathbf{y}) \cdot \nabla s_\varepsilon - \varepsilon^2 \operatorname{div} (\mathbb{D}(\mathbf{y}) : \nabla \nabla s_\varepsilon) \right) &= r && \text{in } \Omega, \\
 \left[\varepsilon^2 \mathbb{D}(\mathbf{y}) : \nabla \nabla s_\varepsilon \right] : [\mathbf{n} \otimes \mathbf{n}] &= 0 && \text{on } \partial\Omega, \\
 s_\varepsilon(\mathbf{x}) &= 0 && \text{on } \bar{\partial}\Omega,
 \end{aligned} \tag{13}$$

where r is a macroscopic source term, and the conductivity \mathbf{K} and the spatial retardation \mathbb{D} are bounded and uniformly elliptic tensors to ensure existence and uniqueness of the solution to the high-order system Nika and Muntean [2024]. In this thesis, we assume the conductivity tensor to be $\mathbf{K}_{ij} = \rho \delta_{ij}$, where $\rho = \rho(\mathbf{y})$ describes the conductivity of the microscopic material. Introducing a length-scale parameter γ_m depending on the number of microstructures in the microscopic cell, we expand the spatial retardation tensor \mathbb{D} to scale with $\gamma_m^2 \rho$.

To describe the link between the microscopic and macroscopic behavior of the

high-order system at steady-state, two-scale expansion is performed [Bensoussan et al., 1978, Sanchez-Palencia, 1980, Bakhvalov and Panasenko, 1989, Mei and Vernescu, 2010]. At microscopic level, for $j = 1, 2$ and $\mathbf{e}_j \in \mathbb{R}^2$ unit vector in the j th direction, the corrector term w^j is the solution to the j th cell problem

$$\begin{aligned} -\operatorname{div}_y \left(\rho(\mathbf{e}_j + \nabla w^j(\mathbf{y})) - \operatorname{div}_y(\gamma_m^2 \rho \nabla_y \nabla_y w^j(\mathbf{y})) \right) &= 0 && \text{in } Y_m, \\ w^j(\mathbf{y}) & && \text{periodic in } Y_m. \end{aligned} \quad (14)$$

Here, the corrector w^j has zero average over the cell Y_m to ensure uniqueness of the solution. Thus, the macroscopic problem is

$$\begin{aligned} -\operatorname{div}_x \left(\mathbf{K}^{\text{eff}} \nabla_x s \right) &= r && \text{in } \Omega, \\ s(\mathbf{x}) &= 0 && \text{on } \partial\Omega, \end{aligned} \quad (15)$$

where s is the macroscopic entropy density, and \mathbf{K}^{eff} is the tensor describing the effective conductivity of the homogenized medium. Namely, the ij th entry of the effective conductivity tensor \mathbf{K}^{eff} is

$$k_{ij}^{\text{eff}} = \frac{1}{|Y_m|} \int_{Y_m} \rho \left(\delta_{ij} + \frac{\partial w^j}{\partial y_i} \right). \quad (16)$$

Note that the corrector terms w^j transfer the relevant microscopic information on the behavior of the heterogeneous medium to the macroscopic equation.

6.3 Numerical Modeling

In this section, we explore how to build a suitable finite element approximation to solve cell problem (14), which in its weak form reads: find $w^j \in U$ such that

$$\int_{Y_m} \rho(\mathbf{e}_j + \nabla w^j) \cdot \nabla \phi + \int_{Y_m} \rho \gamma_m^2 \nabla \nabla w^j : \nabla \nabla \phi = 0 \quad \forall \phi \in U, \quad (17)$$

for U and ϕ appropriate function space and test function, respectively.

To numerically solve cell problems (14), ensuring sufficient regularity of the approximation, we employ tensor product biquadratic B-splines [Prenter, 1975, Höllig, 2003]. While this tensor product structure does not explore the full potential of multivariate features of B-splines [Dahmen, 1980], in our case, it provides a simple and effective way to construct the basis functions and to compute their derivatives in a univariate way.

Here, we consider only a part $Y^{(m)} \subset \mathbb{R}^2$ of the cell that contains only one microstructure, that is, $Y^{(m)} = Y_1$ if $m = 1$, or a portion of Y_m if $m > 1$. To implement a B-spline-based finite element solver for variational cell problem (17), we divide the domain $Y^{(m)}$ into $n = n_{y_1}^2$ square elements E_1, E_2, \dots, E_n of side h . Let $\mathbf{y} \in Y$, and let $B_{e,h}(\mathbf{y})$ be a tensor product biquadratic B-spline centered at element E_e supported on a square interval of side $3h$. The test and trial spaces are

defined as the set of all the linear combinations of the biquadratic B-splines over $Y^{(m)}$, that is,

$$\mathbb{B}_h(Y^{(m)}) = \text{span}_{e \in \{1, 2, \dots, n\}} \{B_{e,h}(\mathbf{y})\}. \quad (18)$$

Moreover, the periodic boundary conditions in cell problem (14) must be incorporated into the construction of the above space. This is achieved by extending the B-splines' support across the periodic boundaries. Finally, the approximation of the solutions w_h^j , $j = 1, 2$, is given by

$$w_h^j(\mathbf{y}) = \sum_{e=1}^n d_e^j B_{e,h}(\mathbf{y}), \quad (19)$$

where d_e^j are the coefficients to be determined.

For $\mathbf{d}^j \in \mathbb{R}^n$ vector of the unknown coefficients d_e^j and $\mathbf{1} = (1, 1, \dots, 1)^T \in \mathbb{R}^n$, the matrix form of variational cell problem (17) is

$$\begin{bmatrix} \mathbf{S} + \mathbf{D} & \mathbf{1} \\ \mathbf{1}^T & 0 \end{bmatrix} \begin{bmatrix} \mathbf{d}^j \\ \lambda \end{bmatrix} = \begin{bmatrix} \mathbf{f}^j \\ 0 \end{bmatrix}, \quad (20)$$

where, $\mathbf{S} \in \mathbb{R}^{n \times n}$ is the stiffness matrix, $\mathbf{D} \in \mathbb{R}^{n \times n}$ is the spatial retardation matrix, $\mathbf{f}^j \in \mathbb{R}^n$ is the right-hand side vector, and λ is a Lagrange multiplier to enforce the periodic boundary condition. Note that, differently from classical finite element methods, here the linear system is expressed in terms of the node free parameters d_e^j instead of nodal values, which can easily be recovered [Gardner and Gardner, 1995].

Denoting by ρ_e the conductivity of element E_e , the stiffness matrix \mathbf{S} , the spatial retardation matrix \mathbf{D} , and the right-hand side vector \mathbf{f}^j have entries,

$$s_{kl} = \sum_{e=1}^n \rho_e \underbrace{\int_{E_e} \nabla B_{k,h} \cdot \nabla B_{l,h}}_{s_{kl}^e}, \quad (21)$$

$$d_{kl} = \sum_{e=1}^n \rho_e \underbrace{\int_{E_e} \gamma_m^2 \nabla \nabla B_{k,h} : \nabla \nabla B_{l,h}}_{d_{kl}^e}, \quad (22)$$

and

$$f_k^j = \sum_{e=1}^n \rho_e \underbrace{\left(- \int_{E_e} \mathbf{e}_j \cdot \nabla B_{k,h} \right)}_{f_k^{j,e}}, \quad i = 1, 2, \quad (23)$$

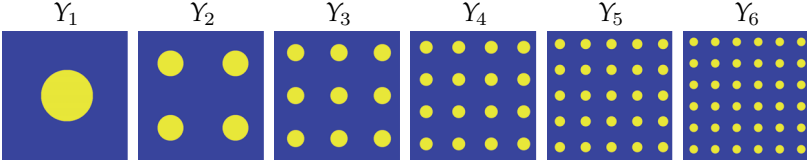


Figure 13: Periodic unit cells Y_m , for $m = 1, \dots, 5$, containing the circular microstructure with different characteristic size. Each unit cell contains $m \times m$ scaled versions of the circular microstructure. The yellow portion indicates a high conductivity κ_c , the blue portion indicates a low conductivity κ_i . Figure from Paper V.

respectively. Lastly, we introduce the mass matrix M having entries

$$m_{kl} = \sum_{e=1}^n \underbrace{\int_{E_e} B_{k,h} B_{l,h}}_{m_{kl}^e}, \quad (24)$$

which we use later on in this thesis.

6.4 Selected Results

All simulations are performed on the square domain $Y^{(m)}$, containing a single microstructure. If not otherwise specified, we discretize the square domain $Y^{(m)}$ into a uniform grid with $n = 512 \times 512$ elements. The simulated microstructure has the following properties: a circular region holding high-conductivity material ($\rho = \kappa_c = 250$), and its complement holding low-conductivity material ($\rho = \kappa_i = 0.2$). Figure 13 shows, from left to right, the different domains Y_m , $m = 1, \dots, 5$, each incorporating circular microstructures with different absolute sizes of the constituents. Here, the yellow portion indicates a high conductivity, while the blue portion indicates a low conductivity. In the limit case $m \rightarrow \infty$, the problem reduces to the classical homogenization scenario, and we denote the portion of the domain containing one microstructure by $Y^{(\infty)}$.

To assess the convergence of the proposed finite element discretization, we numerically solve the problem on $Y^{(m)}$, for a sequence of refined meshes. To avoid artifacts arising from the geometry of the discretized domain, we test convergence on a square microstructure occupying $1/4$ of the area ($1/2$ of each side) of $Y^{(m)}$. Then, we discretize $Y^{(m)}$ into a uniform grid with $n = 2^k \times 2^k$ elements for $m = 1, 2, \dots, 5$ and $k = 4, 5, \dots, 10$. The reference solution is computed with $k = 10$. Figure 14 shows the difference between the computed and the reference solutions in terms of the L^2 (left) and H^2 (right) norms. The results in the figure suggest the following convergence rates:

$$\|u_k - u_{\text{ref}}\|_{H^2} \sim h^{0.7} \quad \text{and} \quad \|u_k - u_{\text{ref}}\|_{L^2} \sim h^{1.3}. \quad (25)$$

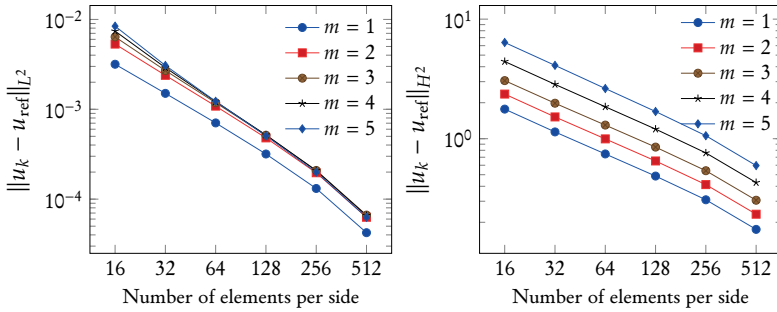


Figure 14: L^2 and H^2 errors for the problem on $Y^{(m)}$, $m = 1, 2, \dots, 5$. Figure from Paper V.

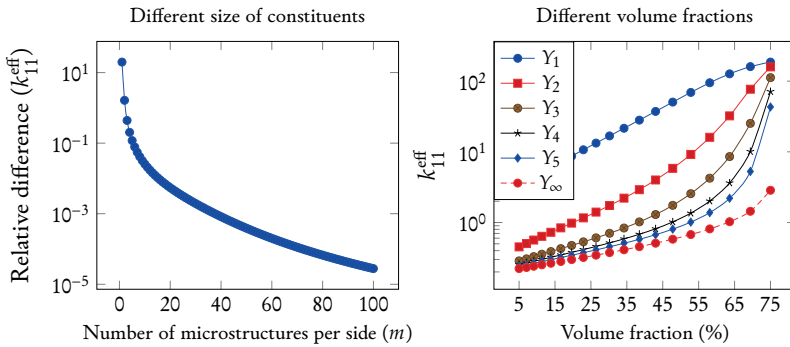


Figure 15: Two numerical experiments: on the left, the relative difference in k_{11}^{eff} between scale-dependent case (with $m = 1, \dots, 100$ microstructures per side) and the classical homogenization ($m \rightarrow \infty$); on the right, the impact of different volume fractions on k_{11}^{eff} with varying length-scales. Figure from Paper V.

This study agrees with the theory: the regularity of the solution is limited by the presence of discontinuous conductivity and re-entrant corners in the low-conductivity region, forming a Kondrat'ev-type singularity [Dauge, 1988].

Figure 15 shows two numerical experiments. On the left, we plot the relative difference between the scale-dependent case containing $m = 1, \dots, 100$ microstructures per side, and the classical homogenization ($m \rightarrow \infty$), in terms of the effective conductivity k_{11}^{eff} . As anticipated, the effective property for the scale-dependent case converges to the classical homogenization case when increasing the number of microstructures in the periodic cell. On the right, we illustrate how scale-size effects alter the curve describing the change in the effective conductivity k_{11}^{eff} for different volume fractions.

Lastly, Figure 16 displays the scale-size effects, in terms of the corrector w^1 , on microstructures with varying volume fractions (5%, 40%, and 75%). The tested domains are $Y^{(m)}$, $m = 1, \dots, 5$ and the classical homogenization case ($m \rightarrow \infty$). This result demonstrates the meaning behind the name *spatial retardation* given to

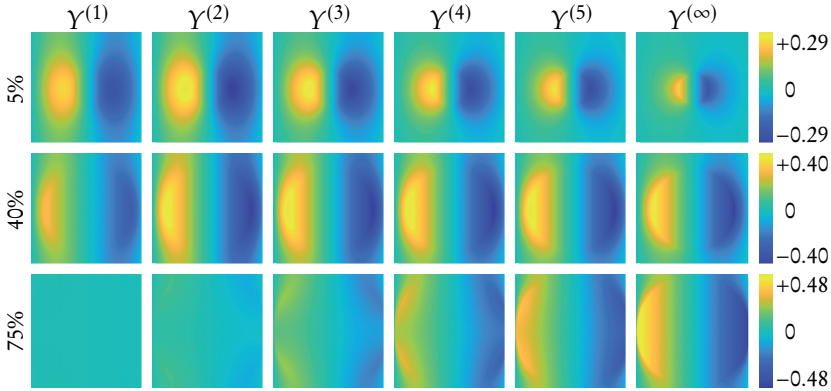


Figure 16: Local solutions w^1 computed for the circular microstructure with varying volume fractions (5 %, 40 %, and 75 %) on microstructure cells $Y^{(m)}$, $m = 1, \dots, 5$ and for the classical homogenization case ($m \rightarrow \infty$). Figure from Paper V.

the second-gradient tensor \mathbb{D} , as the solution field appears less smeared the more microstructures we add to the periodic cell.

7 Optimization of Scale-Size Dependent Microstructures

After learning how scale-size effects influence the effective conductivity of fixed microstructures, one could ask an inverse question: how can we achieve, for a fixed length scale, a predefined effective conductivity by altering the microstructure?

In this section, we explore this particular example of topology optimization tailored for microstructures under the assumption of scale-size effects characteristic of the physics described in Section 6. This section presents a novel extension of what was published in Paper V and is part of an article currently in preparation.

7.1 Problem Formulation

The problem we tackle is to match target values for the effective conductivity of the homogenized medium subject to the enhanced heat equation, while minimizing the volume fraction of the used good conductor. Consider the effective conductivity (16) and a target conductivity tensor $\mathbf{K}^t \in \mathbb{R}^{2 \times 2}$, such that its entries k_{ij}^t form a feasible target tensor [Milton, 2022]. Then, the problem reads: find the best material distribution ρ over the design domain Y_m such that:

$$\begin{cases} \min & \frac{1}{2} \sum_{i,j} (k_{ij}^{\text{eff}} - k_{ij}^t)^2 + \frac{1}{|Y_m|} \int_{Y_m} \rho \\ \text{subject to} & \text{variational cell problem (17),} \\ & 0 \leq \rho \leq 1. \end{cases} \quad (26)$$

This specific formulation can be efficiently solved by taking advantage of the way the Method of Moving Asymptotes (MMA) is structured [Svanberg, 1987].

7.2 Sensitivity analysis

We claim that variational cell problem (17) is self-adjoint. In the following part, we shall prove this claim. Let us divide the objective function into two summable parts as follows:

$$J_c = \frac{1}{2} \sum_{i,j} (k_{ij}^{\text{eff}} - k_{ij}^t)^2, \quad (27)$$

$$J_v = \frac{1}{|Y_m|} \int_{Y_m} \rho. \quad (28)$$

The sensitivity of J_v with respect to perturbations of ρ is trivial. For the other component, more care is required when differentiating the effective conductivity term.

We start by perturbing ρ in the direction $D\rho$. Looking at the first variation of the ij th component of the effective conductivity yields

$$Dk_{ij}^{\text{eff}} = \frac{1}{|Y_m|} \int_{Y_m} D\rho(\delta_{ij} + \partial_i w^j) + \frac{1}{|Y_m|} \int_{Y_m} \rho \partial_i (Dw^j). \quad (29)$$

To expand the last term of the perturbed effective conductivity, we consider the first variation of the j th direction of variational cell problem (17). , we consider the first variation of the j -th cell problem (17). Rearranging the terms of the perturbed variational problem, we attain

$$\begin{aligned} - \left(\int_{Y_m} D\rho \nabla w^j \cdot \nabla \phi + \int_{Y_m} D\rho \gamma_m^2 \nabla \nabla w^j : \nabla \nabla \phi + \int_{Y_m} D\rho e_j \cdot \nabla \phi \right) = \\ \int_{Y_m} \rho \nabla (Dw^j) \cdot \nabla \phi + \int_{Y_m} \rho \gamma_m^2 \nabla \nabla (Dw^j) : \nabla \nabla \phi \quad \forall \phi \in U. \end{aligned} \quad (30)$$

We now define the adjoint problem as: find λ^i , such that

$$\int_{Y_m} \rho \nabla z \cdot \nabla \lambda^i + \int_{Y_m} \rho \gamma_m^2 \nabla \nabla z : \nabla \nabla \lambda^i = - \frac{1}{|Y_m|} \int_{Y_m} \rho e_i \cdot \nabla z \quad \forall z \in U. \quad (31)$$

Following the properties of variational cell problem (17), we can write the solution to the latter differential equation as

$$\lambda^i = \frac{1}{|Y_m|} w^i. \quad (32)$$

Moreover, selecting $\phi = \lambda^i$ in variational problem (30) yields

$$\begin{aligned} - \left(\int_{Y_m} D\rho \nabla w^j \cdot \nabla \lambda^i + \int_{Y_m} D\rho \gamma_m^2 \nabla \nabla w^j : \nabla \nabla \lambda^i + \int_{Y_m} D\rho e_j \cdot \nabla \lambda^i \right) = \\ \int_{Y_m} \rho \nabla (Dw^j) \cdot \nabla \lambda^i + \int_{Y_m} \rho \gamma_m^2 \nabla \nabla (Dw^j) : \nabla \nabla \lambda^i. \end{aligned} \quad (33)$$

Using the previous relation together with adjoint problem (31), with $z = Dw^j$, we obtain

$$\begin{aligned} \frac{1}{|Y_m|} \int_{Y_m} \rho \partial_i (Dw^j) &= \int_{Y_m} D\rho \nabla w^j \cdot \nabla \lambda^i \\ &+ \int_{Y_m} D\rho \gamma_m^2 \nabla \nabla w^j : \nabla \nabla \lambda^i \\ &+ \int_{Y_m} D\rho e_j \cdot \nabla \lambda^i. \end{aligned} \quad (34)$$

Substituting this result into perturbed effective conductivity (29), and using identity (32), yields

$$\begin{aligned} Dk_{ij}^{\text{eff}} &= \frac{1}{|Y_m|} \int_{Y_m} D\rho (\delta_{ij} + \partial_i w^j) + \frac{1}{|Y_m|} \int_{Y_m} D\rho \nabla w^j \cdot \nabla w^i \\ &+ \frac{1}{|Y_m|} \int_{Y_m} D\rho \gamma_m^2 \nabla \nabla w^j : \nabla \nabla w^i + \frac{1}{|Y_m|} \int_{Y_m} D\rho e_j \cdot \nabla w^i, \end{aligned} \quad (35)$$

which can be reorganized in a more compact form as

$$Dk_{ij}^{\text{eff}} = \frac{1}{|Y_m|} \int_{Y_m} D\rho \left((e_i + \nabla w^i) \cdot (e_j + \nabla w^j) + \nabla \nabla w^i : \nabla \nabla w^j \right). \quad (36)$$

Due to the symmetric and self-adjoint nature of the system, the sensitivities can be assembled efficiently from the available correctors w^i and the precomputed element matrices, without the need to solve any additional equations. Following the notation of Section 6.3, we discretize the domain $Y^{(m)}$ into $n = n_{y_1}^2$ square elements of side h . Writing the solution in its approximate form d^i , as in (19), the sensitivity for an element E_e can be identified as

$$\frac{dJ_c}{d\rho_e} = \frac{1}{|Y_m|} \sum_{i,j} (k_{ij}^{\text{eff}} - k_{ij}^t) \left(\delta_{ij} M_e + f_e^i d_e^j + f_e^j d_e^i + d_e^i (S_e + D_e) d_e^j \right), \quad (37)$$

where f_e^i is the right-hand side vector defined in (23), and M_e , S_e , and D_e are the element matrices defined in (24), (21), and (22), respectively.

7.3 Selected Results

To solve optimization problem (26), we employ the notation and modeling described in Section 6. However, in this section, the unitary square domain $Y^{(m)}$ containing a single microstructure is discretized into 128×128 square elements, and the microscopic conductivity is replaced by its SIMP interpolation [Bendsøe, 1989] as

$$P(\rho) = \kappa_i + (\kappa_c - \kappa_i) \rho^p, \quad (38)$$

where the low conductivity is $\kappa_i = 0.001$, the high conductivity is $\kappa_c = 1$, $p \geq 1$ is a penalization parameter. To impose minimum size control in the microstructures, we employ a heuristic inspired by the one presented in Section 3 using fW -mean

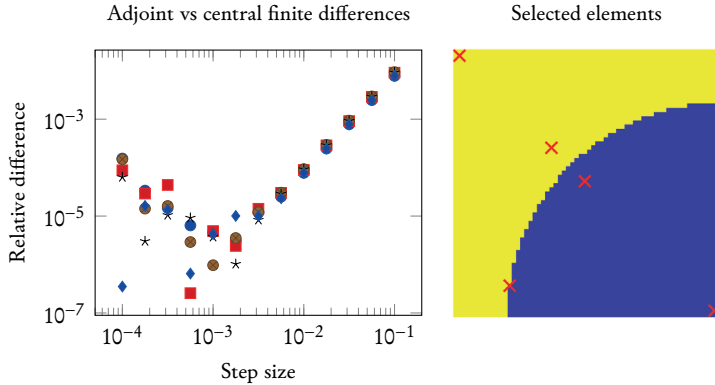


Figure 17: Relative difference (left) between the sensitivities $dJ_c/d\rho_e$ computed with the adjoint method and with finite differences for different step sizes for some selected elements (right). The elements are picked from the top-left quadrant of the domain Y_1 containing a circular microstructure, as described by Figure 13.

filters [Wadbro and Hägg, 2015] with a filter radius of $1/32$, corresponding to 4 elements in the chosen discretization. In this case, the first term of the objective function, J_c , is computed using the open filtered design, while the volume term, J_v , is computed using the closed filtered design. A continuation method is applied to promote a grey-scale-free final design by increasing the penalization p and decreasing the filter non-linearity parameter α until $p = 7$ and $\alpha = 10^{-8}$. The chosen initial guess for all the optimization experiments is a circular microstructure occupying half of the design domain.

To assess the accuracy of the derived sensitivities, let us consider the domain Y_1 containing a circular microstructure with a volume fraction of 0.5 similar to the one in Figure 13, and let us select some relevant elements—namely, in the proximity of the center of the microstructure, the corner of the domain, and the jump in conductivity. On the selected elements, we compare the sensitivities derived with the adjoint method in (17) with the ones computed using a central finite differences scheme. Figure 17 plots the relative difference between the two methods against the step size of the finite differences (on the left), and the selected elements with red crosses (on the right). The displayed accuracy aligns with what is expected.

In the first numerical experiments, we target isotropic structures. Namely, the target conductivity tensors are $k_{ij}^t = 0.2\delta_{ij}$ and $k_{ij}^t = 0.4\delta_{ij}$. Figures 18 and 19 show the resulting isotropic designs for the tested microscopic cells $Y^{(m)}$ in the scale-dependent cases $m = 1, 2, 3$ and for the classical homogenization case ($m \rightarrow \infty$).

Successively, anisotropic structures are targeted. In this case, the target indicates a higher conductivity in one axial direction or a rotated version of the properties.

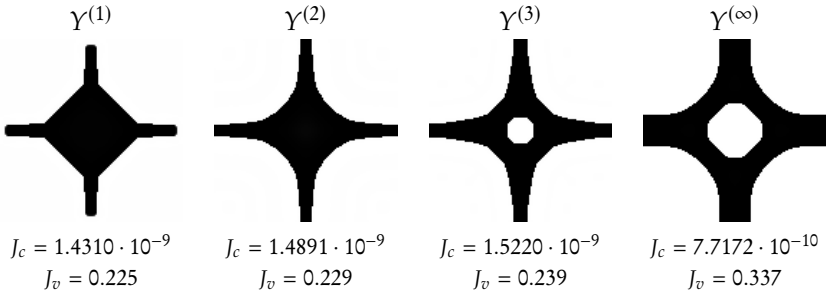


Figure 18: Final designs for the target $k_{ij}^t = 0.2\delta_{ij}$ and zero elsewhere, with respective objective values, on the microscopic cells $\Upsilon^{(m)}$, $m = 1, 2, 3$ and for the classical homogenization case ($m \rightarrow \infty$).

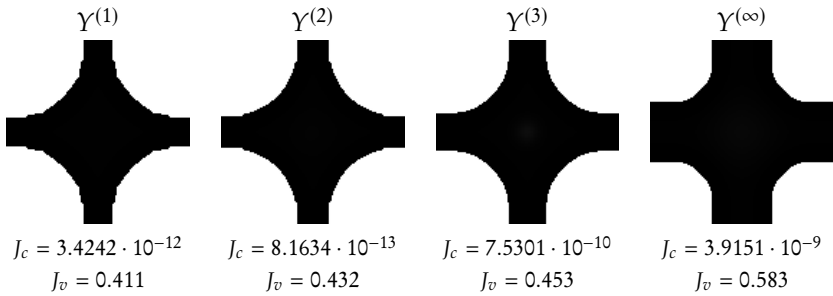


Figure 19: Final designs for the target $k_{ij}^t = 0.4\delta_{ij}$ and zero elsewhere, with respective objective values, on the microscopic cells $\Upsilon^{(m)}$, $m = 1, 2, 3$ and for the classical homogenization case ($m \rightarrow \infty$).

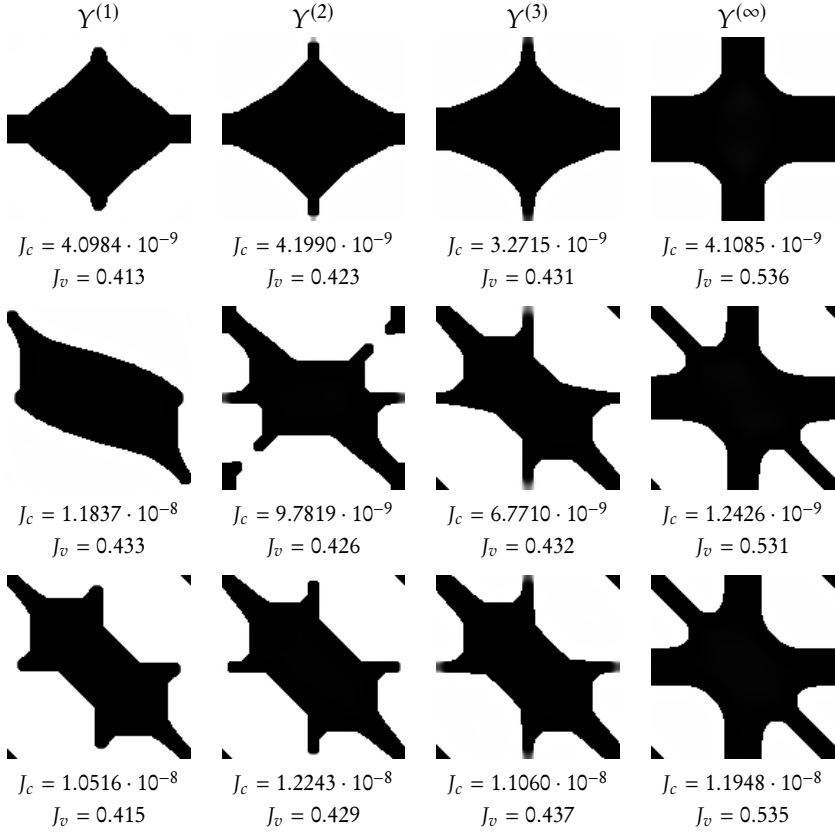


Figure 20: Final designs for the anisotropic target having components $k_{11}^t = 0.4$, $k_{22}^t = 0.3$ and zero elsewhere, with respective objective values, on the microscopic cells $Y^{(m)}$, $m = 1, 2, 3$ and for the classical homogenization case ($m \rightarrow \infty$). The rows (top to bottom) show the unrotated properties, and the ones rotated clockwise by 30° and 45° , respectively.

The specific targets we test are

$$K^t = \begin{pmatrix} 0.4 & 0 \\ 0 & 0.3 \end{pmatrix}, \begin{pmatrix} 0.3750 & 0.0433 \\ 0.0433 & 0.3250 \end{pmatrix}, \text{ or } \begin{pmatrix} 0.35 & 0.05 \\ 0.05 & 0.35 \end{pmatrix}, \quad (39)$$

where the second and the third target a 30° and 45° clockwise rotation, respectively, of the properties in the first target. Figure 20 depicts these simulations. Specifically, the topmost row refers to the unrotated properties, while the second and third rows refer to those rotated clockwise by 30° and 45° , respectively.

Overall, the numerical results exhibit the feasibility of the problem: the low values of the objective portion J_c suggest that the target values are met. As for the volume fraction, while it is being minimized over the domains $Y^{(m)}$, we mostly notice an increasing trend when comparing the periodic cells Y_m for different

values of m . This volume increase follows the logic: a consequence of the *spatial retardation* term seen in Section 6 is that the gradients of the local solutions to the governing equations get sharper when increasing the number of microstructures per cell. Consequently, the optimizer may place more material, since the correctors w^i peak over a narrower surface as m increases. Upon visual inspection of the results, the designs optimized over $Y^{(m)}$ show, as m increases, a converging trend towards the design in $Y^{(\infty)}$. The convergence of the scale-dependent model to the classical homogenization case is consistent with the behavior observed in Figure 15.

Finally, a visible issue in some designs is the presence of gray areas. These are preliminary results; these cases are currently under investigation. In parallel, more numerical experiments are being executed. While testing different target values, we aim to investigate how the initial design affects the final results.

8 Concluding Remarks and Future Work

This thesis designed and tested techniques for topology optimization, with a focus on boundary-aware and multiscale formulations. Specifically, by investigating the research questions posed in Section 1.1, we contributed to the development of a broader topology optimization framework on two fronts: boundary-aware approaches for coated structures, and microstructured materials with scale-size effects.

Regarding boundary-aware formulations, the main contribution of this thesis is the introduction of a boundary strip indicator inspired by mathematical morphology. For material distribution-based topology optimization, the indicator provides a consistent tool to identify and control a coating layer in the design. The indicator is tested numerically on a compliance problem with two different methods—one employing binary design variables, one allowing intermediate values. Numerical results demonstrate the influence of the coating layer’s properties on the optimized designs.

In parallel, a computational framework for the topology optimization of rigid microstructures with scale-size effects is developed. By combining the introduction of a scale-dependent term with homogenization techniques and a suitable numerical approximation, the thesis shows how characteristic size directly impacts effective properties and optimal layouts. The numerical results highlight the need for scale-dependent terms when designing system components that approach the nanoscale.

Conclusively, the thesis showed the relevance of boundary-aware formulations and scale-dependent modeling in material distribution-based topology optimization, specifically in the context of coated structures and microstructured materials with scale-size effects. As in many modern design problems, the optimized designs are strongly affected by the geometry and physics of the systems. Thus, accurately capturing boundary layers and size effects is crucial for obtaining physically meaningful and reliable optimized designs.

Several directions for future studies naturally emerge from this thesis. For boundary-aware formulations, extensions to more complex interfaces and mul-

tiphysics settings are promising directions. An example of complex interface problems could be formulated by introducing multi-layered materials with variable layer thickness. In the context of multiscale formulations, including transient, multiphysics, and boundary-dependent phenomena would broaden the applicability of the proposed scale-dependent approach. Particularly, the above potential developments could benefit from an extended multi-material formulation. Overall, these further studies would contribute to extending topology optimization towards a more comprehensive framework. As engineering systems continue to evolve towards smaller scales and increased complexity, such approaches will open new possibilities in designing the next generation of optimized metamaterials and structures.

List of Appended Papers

1. Rômulo L. Cortez, Mario Setta, Renato Picelli, Eddie Wadbro. Minimum size control for binary topology optimization. *Struct Multidisc Optim* **68**, 34 (2025). DOI: 10.1007/s00158-025-03975-3.
2. Mario Setta, Linus Hägg, Eddie Wadbro. A boundary strip indicator for material distribution-based topology optimization. *Struct Multidisc Optim* **67**, 149 (2024). DOI: 10.1007/s00158-024-03872-1.
3. Mario Setta, Rômulo L. Cortez, Renato Picelli, Eddie Wadbro. Binary topology optimization for coated structures. *Struct Multidisc Optim* **68**, 173 (2025). DOI: 10.1007/s00158-025-04103-x.
4. Eddie Wadbro, Quoc Khanh Nguyen, Mario Setta, Martin Berggren, Abbas Mousavi. Material distribution topology optimization for boundary-effect-dominated problems: a review. *Struct Multidisc Optim* **69**, 102 (2026). DOI: 10.1007/s00158-026-04287-w.
5. Mario Setta, Grigor Nika, Eddie Wadbro. Simulation of effective scale-size dependent heat conduction in rigid microgeometries. *Computer Methods in Applied Mechanics and Engineering*, 452 (2026), pp.118752. DOI: 10.1016/j.cma.2026.118752.

Comments on my Participation

Paper I I contributed to the study of the proposed method and to its implementation on MATLAB. I contributed to the initial draft of the manuscript. I was supported by all the co-authors on theory, numerical simulations, drafting, and revising. Rômulo L. Cortez and I contributed equally to the development of this paper. I was responsible for the submission process and for the correspondence with the journal editor.

Paper II I contributed to the study of the proposed method, and I implemented it on MATLAB. I was responsible for the numerical simulations and for the writing of the initial draft of the manuscript. I was supported by all the co-authors on theory, numerical simulations, drafting, and revising. I was responsible for the submission process and for the correspondence with the journal editor.

Paper III I contributed to the study of the proposed method and to its implementation on MATLAB. I was responsible for the numerical simulations and for writing most of the initial draft of the manuscript. I was supported by all the co-authors on theory, numerical simulations, drafting, and revising. Rômulo L. Cortez and I contributed equally to the development of this paper. I was responsible for the submission process and for the correspondence with the journal editor.

Paper IV I contributed to the search and study of the presented articles. I led the statistics research and the writing of the section on coated structures. I contributed to the writing and editing of the other sections. I was supported by all the co-authors on theory, drafting, and revising.

Paper V I contributed to the study of the proposed method and to its implementation on MATLAB. I was responsible for the numerical simulations and for writing the homogenization, numerical treatment, and simulation parts of the initial draft of the manuscript. I was supported by all the co-authors on theory, numerical simulations, drafting, and revising.

References

- N. Bakhvalov and G. Panasenko. *Homogenisation: averaging processes in periodic media: mathematical problems in the mechanics of composite materials*. Kluwer Academic Publishers, 1989.
- J. Bauer, L. R. Meza, T. Schaedler, R. Schwaiger, X. Zheng, and L. Valdevit. Nanolattices: an emerging class of mechanical metamaterials. *Advanced Materials*, 29(40):1701850, 2017. doi: 10.1002/adma.201701850.
- M. Bendsøe. *Optimization of Structural Topology, Shape, and Material*. Springer Verlag, Germany, 2013. ISBN 978-3-662-03115-5.
- M. Bendsøe and O. Sigmund. *Topology Optimization: Theory, Methods, and Applications*. Springer Verlag, Germany, 2003. ISBN 3-540-42992-1.
- M. P. Bendsøe. Optimal shape design as a material distribution problem. *Structural optimization*, 1(4):193–202, 1989. doi: 10.1007/BF01650949.
- M. P. Bendsøe and N. Kikuchi. Generating optimal topologies in structural design using a homogenization method. *Computer Methods in Applied Mechanics and Engineering*, 71(2):197–224, 1988. doi: 10.1016/0045-7825(88)90086-2.
- A. Bensoussan, J.-L. Lions, and G. Papanicolaou. *Asymptotic Analysis for Periodic Structures*. AMS Chelsea Publishing, Providence, RI, 1978.
- T. Borrvall. Topology optimization of elastic continua using restriction. *Archives of Computational Methods in Engineering*, 8:351–385, 2001. doi: 10.1007/BF02743737.
- T. E. Bruns and D. A. Tortorelli. Topology optimization of non-linear elastic structures and compliant mechanisms. *Computer Methods in Applied Mechanics and Engineering*, 190(26):3443–3459, 2001. doi: 10.1016/S0045-7825(00)00278-4.
- C. Christov. On a higher-gradient generalization of Fourier’s law of heat conduction. In *AIP Conference Proceedings*, volume 946(1), pages 11–22. American Institute of Physics, 2007. doi: 10.1063/1.2806035.
- A. Clausen, N. Aage, and O. Sigmund. Topology optimization of coated structures and material interface problems. *Comput. Methods Appl. Mech. Engrg.*, 290: 524–541, 2015. doi: 10.1016/j.cma.2015.02.011.
- W. Dahmen. On multivariate B-Splines. *SIAM J. Numer. Anal.*, 17(2):179–191, 1980. ISSN 00361429. doi: 10.1137/0717017.
- M. Dauge. *Elliptic Boundary Value Problems on Corner Domains*. Springer Berlin, Heidelberg, 1988. doi: 10.1007/BFb0086682.
- S. Forest and M. Amestoy. Hypertemperature in thermoelastic solids. *C. R. Méc.*, 336(4):347–353, 2008. doi: 10.1016/j.crme.2008.01.007.

- S. Forest, F. Pradel, and K. Sab. Asymptotic analysis of heterogeneous Cosserat media. *Int. J. Solids Structures*, 38(26-27):4585–4608, 2001. doi: 10.1016/S0020-7683(00)00295-X.
- J.-F. Ganghoffer, X. N. Do, and S. Fumeron. Emergence of anomalous hyperbolic heat conduction in homogenized media. *Compos. Struct.*, page 119492, 2025a. doi: 10.1016/j.compstruct.2025.119492.
- J.-F. Ganghoffer, X. N. Do, and I. Goda. Surface and size effects in architected materials via first strain gradient theory. *Int. J. Mech. Sci.*, page 111021, 2025b. doi: 10.1016/j.ijmecsci.2025.111021.
- L. Gardner and G. Gardner. A two dimensional bi-cubic b-spline finite element: used in a study of mhd-duct flow. *Computer Methods in Applied Mechanics and Engineering*, 124(4):365–375, 1995. ISSN 0045-7825. doi: 10.1016/0045-7825(94)00760-K.
- M. Gurtin. Generalized Ginzburg-Landau and Cahn-Hilliard equations based on a microforce balance. *Phys. D*, 92(3-4):178–192, 1996. doi: 10.1184/R1/6477524.
- L. Hägg and E. Wadbro. On minimum length scale control in density based topology optimization. *Structural and Multidisciplinary Optimization*, 58:1015–1032, 2018. doi: 10.1007/s00158-018-1944-0.
- K. Höllig. *Finite Element Methods with B-Splines*. Society for Industrial and Applied Mathematics, 2003. doi: 10.1137/1.9780898717532.
- IBM Corporation. *IBM ILOG CPLEX Optimization Studio V22.1: User's Manual for CPLEX*. International Business Machines Corporation, Armonk, NY, 2022.
- M. Kadic, T. Frenzel, and M. Wegener. When size matters. *Nature Physics*, 14(1): 8–9, 2018. doi: 10.1038/nphys4287.
- R. V. Kohn and G. Strang. Optimal design and relaxation of variational problems, I. *Comm. Pure Appl. Math.*, 39(1):113–137, 1986a. doi: 10.1002/cpa.3160390107.
- R. V. Kohn and G. Strang. Optimal design and relaxation of variational problems, II. *Comm. Pure Appl. Math.*, 39(2):139–182, 1986b. doi: 10.1002/cpa.3160390202.
- R. V. Kohn and G. Strang. Optimal design and relaxation of variational problems, III. *Comm. Pure Appl. Math.*, 39(3):353–377, 1986c. doi: 10.1002/cpa.3160390305.
- Y. Liang and G. Cheng. Topology optimization via sequential integer programming and canonical relaxation algorithm. *Computer Methods in Applied Mechanics and Engineering*, 348:64–96, 2019. doi: 10.1016/j.cma.2018.10.050.

- J. L. Lions. *Optimal control of systems governed by partial differential equations*, volume 170 of *Die Grundlehren der mathematischen Wissenschaften*. Springer, Berlin, 1971. Translated by S. K. Mitter.
- G. Matheron. *Random Sets and Integral Geometry*. Wiley Series in Probability and Mathematical Statistics. Wiley, New York, 1974.
- C. C. Mei and B. Vernescu. *Homogenization Methods for Multiscale Mechanics*. World Scientific, 2010.
- G. W. Milton. *The Theory of Composites*. Society for Industrial and Applied Mathematics, Philadelphia, PA, 2022. doi: 10.1137/1.9781611977486.
- H. Minkowski. Volumen und oberfläche. *Mathematische Annalen*, 57:447–495, 1903. doi: 10.1007/BF01445180.
- D. Molavitabrizi, S. Khakalo, R. Bengtsson, and S. Mousavi. Second-order homogenization of 3-D lattice materials towards strain gradient media: numerical modelling and experimental verification. *Cont. Mechanics & Thermodyn.*, pages 1–20, 2023. doi: 10.1007/s00161-023-01246-4.
- G. Nika and A. Muntean. Effective medium theory for second-gradient elasticity with chirality. *Asym. Analysis*, 139(1-2):111–137, 2024. doi: 10.48550/arXiv.2202.00644.
- W. Noll and B. Coleman. The thermodynamics of elastic materials with heat conduction and viscosity. In W. Noll, editor, *The Foundations of Mechanics and Thermodynamics: Selected Papers*, pages 145–156. Springer, 1974. doi: 10.1007/BF01262690.
- J. A. Postigo, A. Garaigordobil, R. Ansola, and J. Canales. Topology optimization of shell–infill structures with enhanced edge-detection and coating thickness control. *Adv. Eng. Softw.*, 189:103587, 2024. doi: 10.1016/j.advengsoft.2023.103587.
- W. K. Pratt. *Digital Image Processing*. Wiley, New York, 1991. ISBN 978-0-471-76777-0.
- P. Prenter. *Splines and variational methods*. Wiley, New York, 1975.
- O. Querin, G. Steven, and Y. Xie. Evolutionary structural optimisation (eso) using a bidirectional algorithm. *Engrg. Comput.*, 15(8):1031–1048, 1998. doi: 10.1108/02644409810244129.
- L. Rabiner. Combinatorial optimization: algorithms and complexity. *IEEE Transactions on Acoustics, Speech, and Signal Processing*, 32(6):1258–1259, 1984. doi: 10.1109/TASSP.1984.1164450.
- E. Sanchez-Palencia. *Non-homogeneous media and vibration theory*. Springer-Verlag Berlin Heidelberg, 1980. doi: 10.1007/3-540-10000-8.

- O. Sigmund. *Design of material structures using topology optimization*. PhD thesis, Technical University of Denmark, 1994.
- O. Sigmund. A 99 line topology optimization code written in matlab. *Structural and Multidisciplinary Optimization*, 21(2):120–127, 2001. doi: 10.1007/s001580050176.
- O. Sigmund. Morphology-based black and white filters for topology optimization. *Structural and Multidisciplinary Optimization*, 33:401–424, 2007. doi: 10.1007/s00158-006-0087-x.
- R. Sivapuram and R. Picelli. Topology optimization of binary structures using integer linear programming. *Finite Elements in Analysis and Design*, 139:49–61, 2018. doi: 10.1016/j.finel.2017.10.006.
- S. M. Smith and J. M. Brady. SUSAN—A new approach to low level image processing. *Int. J. Comput. Vision*, 23(1):45–78, 1997. doi: 10.1023/A:1007963824710.
- K. Svanberg. The method of moving asymptotes—a new method for structural optimization. *International Journal for Numerical Methods in Engineering*, 24(2):359–373, 1987. doi: 10.1002/nme.1620240207.
- K. Svanberg. A class of globally convergent optimization methods based on conservative convex separable approximations. *SIAM Journal on Optimization*, 12(2):555–573, 2002. doi: 10.1137/S1052623499362822.
- K. Svanberg and H. Svärd. Density filters for topology optimization based on the pythagorean means. *Structural and Multidisciplinary Optimization*, 48:859–875, 2013. doi: 10.1007/s00158-013-0938-1.
- A. Tovar and K. Khandelwal. Continuation method and filter reduction in global topology optimization. In *International Conference on Computer Methods in Mechanics (CMM 2011)*, May 2011.
- E. Wadbro and L. Hägg. On quasi-arithmetic mean based filters and their fast evaluation for large-scale topology optimization. *Structural and Multidisciplinary Optimization*, 52:879–888, 2015. doi: 10.1007/s00158-015-1273-5.
- W. Zhang, W. Zhong, and X. Guo. An explicit length scale control approach in simp-based topology optimization. *Computer Methods in Applied Mechanics and Engineering*, 282:71–86, 2014. doi: 10.1016/j.cma.2014.08.027.



Boundary-Aware and Multiscale Methods for Topology Optimization

This thesis synthesizes recent advances in topology optimization, focusing on boundary-dominated problems and microstructured materials with scale-size effects. We explore results in boundary-aware formulations, specifically for coated structures, and scale-size dependent modeling for topology optimization. Specifically, we propose a boundary strip indicator based on morphological operators as a simple and robust tool for extracting geometric information, such as coating layers, within the density-based topology optimization framework employing binary and continuous design variables. In parallel, we solve a scale-size dependent model based on higher-order homogenization to reveal the critical role of internal length scales in microgeometries, where classical continuum assumptions fail. Numerical experiments display the influence of coated structures and of scale-size-dependent properties on the resulting optimized microstructures.

ISBN 978-91-7867-711-5 (print)

ISBN 978-91-7867-712-2 (pdf)

ISSN 1403-8099

DOCTORAL THESIS | Karlstad University Studies | 2026:31
